Solution Structure of Co(III)-Bleomycin-OOH Bound to a Phosphoglycolate Lesion Containing Oligonucleotide: Implications for Bleomycin-Induced Double-Strand DNA Cleavage†

Silvia T. Hoehn,‡ Hans-Dieter Junker,‡ Richard C. Bunt,‡ Christopher J. Turner,§ and JoAnne Stubbe*,‡,||

Departments of Chemistry and Biology and Francis Bitter Magnet Laboratory, Massachusetts Institute of Technology, 77 Massachusetts Avenue, Cambridge, Massachusetts 02139

Received November 15, 2000; Revised Manuscript Received March 28, 2001

ABSTRACT: Bleomycin (BLM) is an antitumor antibiotic that is used clinically. Its major cause of cytotoxicity is thought to be related to BLM's ability to cause double-strand (ds) DNA cleavage. A single molecule of BLM appears to cleave both strands of DNA in the presence of its required cofactors Fe^{2+} and oxygen without dissociating from the helix. A mechanism for this process has been proposed based on a model structure of the hydroperoxide of Co(III)-BLM (CoBLM) bound sequence-specifically to an intact duplex containing a GTAC site, a hot spot for ds cleavage [Vanderwall, D. E., Lui, S. M., Wu, W., Turner, C. J., Kozarich, J. W., and Stubbe, J. (1997) *Chem. Biol. 4*, 373−387]. In this paper, we present a structural model for the second cleavage event. Two-dimensional NMR spectroscopy and molecular modeling were carried out to study CoBLM bound to d(CCAAAGXACTGGG)·d(CCCAGTACTTTGG), where X represents a 3′-phosphoglycolate lesion next to a 5′-phosphate. Assignments of 729 NOEs, including 51 between the drug and the DNA and 126 within the BLM molecule, have been made. These NOEs in addition to 96 dihedral angle constraints have been used to obtain a well-defined structural model for this complex. The model reveals that the bithiazole tail is partially intercalated between the T19 and the A20 of the duplex and that the metal binding domain is poised for abstraction of the T19 H4′ in the minor groove. The modeling further reveals that the predominant conformation of the bithiazole protons is trans. Two cis conformations of these protons are also observed, and ROESY experiments provide evidence for interconversion of all of these forms. The relationship of these observations to the model for ds cleavage is presented.

The bleomycins (BLMs)[1] are antitumor antibiotics that are used clinically (Figure 1). These natural products were first isolated from *Streptomyces verticillus* and characterized by Umezawa and co-workers in the 1960s (*1, 2*). Usually used in combination chemotherapy, the drug is effective in the treatment of head and neck cancer and Hodgkin's Disease as well as testicular cancer (*3*−*9*). BLM consists of a glycopeptide that is proposed to bind iron and oxygen in vivo to produce activated BLM, an Fe^{3+} hydroperoxide (*10*−*12*). This intermediate subsequently damages DNA in a sequence-specific manner, inducing both single-strand (ss) and double-strand (ds) DNA cleavage (*13*−*19*). The ds cleavage event is rare: 1 such event occurs for every 6−20 ss cleavage events (*20*−*27*). The ds cleavage is thought to be responsible for BLM's cytotoxicity (*28, 29*). In addition to DNA damage, RNA cleavage as well as damage to other

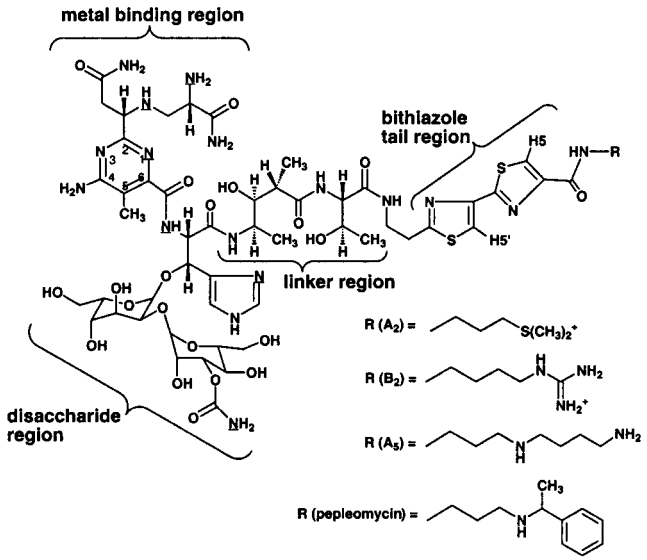

FIGURE 1: Bleomycin. Atoms proposed to be involved in metal binding for different metalloBLMs are underlined.

† This work was supported by NIH Grant GM34454. The NMR facility is supported by NIH Grant RR-00995.

* To whom correspondence should be addressed: telephone (617) 253-1814, fax (617) 258-7247, e-mail stubbe@mit.edu.

‡ Department of Chemistry.

§ Francis Bitter Magnet Laboratory.

|| Department of Biology.

[1] Abbreviations: BLM, bleomycin; ss, single-strand; ds, double-strand; 3′-PG, 3′-phosphoglycolate; 5′-P, 5′-phosphate; CoBLM, Co(III)-hydroperoxide of bleomycin; Pu, purine; Py, pyrimidine; 1D, one-dimensional; 2D; two-dimensional; HAP1, human apurinic/apyrimidinic endonuclease; d, deoxy; A, adenine; C, cytosine; G, guanine; T, thymine; HPLC, high-performance liquid chromatography; TSP, 3-(trimethylsilyl)-1-propanesulfonate; SGI, Silicon Graphics; psf, molecular structure file; TMP, trimethyl phosphate; NOE, nuclear Overhauser effect; IRMA, Iterative Relaxation Matrix Approach; PDB, Protein Data Bank; MD, molecular dynamics; bp, base pair(s).

10.1021/bi002635g CCC: $20.00
Published on Web 04/26/2001

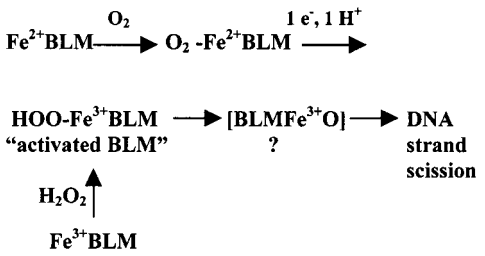

FIGURE 2: BLM activation scheme (*39, 73*).

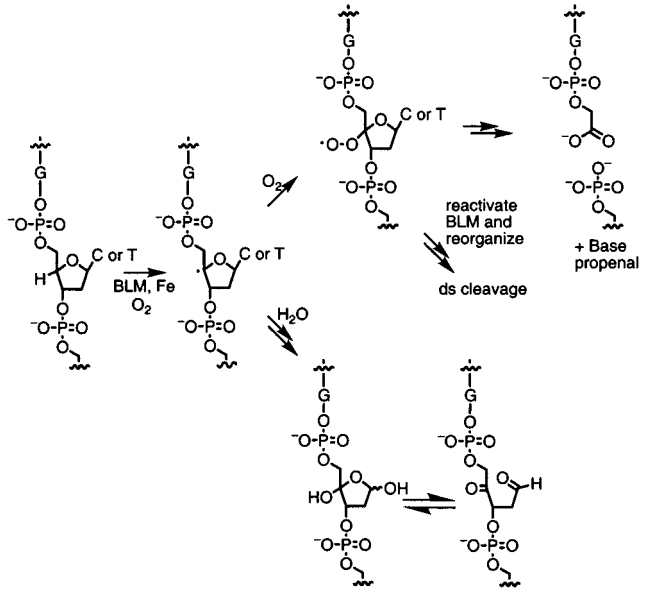

FIGURE 3: Proposed scheme for the formation of the two products resulting from BLM-induced H4′ abstraction. If oxygen adds into the radical, a 3′-PG lesion end, next to a 5′-P end, is generated. Under anaerobic conditions, a 4′-keto abasic site results.

molecules in the cell may also contribute to BLM's cytotoxicity (*30*−*34*). The implication that ds cleavage is responsible for BLM's cytotoxicity has prompted us to carry out structural studies in order to investigate the mechanism of this process.

The mechanism of ds cleavage by a single BLM molecule has been examined in some detail (*18, 19*). BLM is activated in the presence of Fe^{2+}, O_2, and a reductant to generate "activated BLM" (Figure 2) (*10*−*12*). Activated BLM abstracts a 4′-H atom from a pyrimidine 3′ to guanine in duplex DNA (*13*−*17*). After the initial formation of the C4′ radical, two types of lesions result (Figure 3). If the O_2 concentration is high, oxygen reacts with the 4′ sugar radical to eventually generate DNA strand cleavage products including a 3′-phosphoglycolate (3′-PG) end, a 5′-phosphate (5′-P) end, and a base propenal. Under hypoxic conditions, hydroxylation of the C4′ radical occurs, resulting in a 4′-keto abasic site (*14, 35*). Only the pathway leading to the 3′-PG lesion can result in a ds break (*18, 36, 37*).

The present understanding of the chemistry of activated BLM formation requires that for a single BLM to be involved in ds cleavage, it must be reactivated after the initial 4′-H atom abstraction. The chemistry of this reactivation is not understood. We have proposed that the peroxy radical formed by addition of oxygen to the C4′ radical reactivates the spent BLM (Figure 3) (*18, 36*). The reactivated BLM is then proposed to reorganize to the second cleavage site, 15−18 Å away from the initial site of 4′-H atom abstraction, without

5′-G-**Py**-Py-Pu-3′ 5′-G-**Py**-Pu-Py-3′
3′-C-Pu-Pu-Py-5′ 3′-C-Pu-Py-Pu-5′

5′-G-**Py**-Pu-Pu-3′
3′-C-Pu-Py-Py-5′

FIGURE 4: Sequence specificity of ds cleavage (*25*). Boldface type indicates the primary cleavage site; underlines indicate the secondary cleavage site.

dissociating from the helix (*36, 38*). At the secondary cleavage site, BLM again initiates chemistry by 4′-H atom abstraction. This second DNA attack leads to a ds lesion containing either two 3′-PG and 5′-P lesions on opposite strands, or one 3′-PG adjacent to a 5′-P with a 4′-keto abasic site on the second strand (*24*).

Studies from Povirk's lab and our lab suggest that there are hot spots for ds cleavage. A model for the specificity of ds cleavage has been proposed based on the analysis of limited sequence space and is shown in Figure 4 (boldface, primary site of cleavage; underlined, secondary site of cleavage) (*25*). Blunt-ended cleavage and cleavage staggered toward the 5′-side are very unusual for chemistry in the minor groove. Thus, how one molecule of BLM can effect this specificity is of great interest.

There is a general consensus that BLM, which effects its chemistry in the minor groove, can bind by either partial intercalation or binding in the minor groove. However, whether both binding modes can lead to DNA cleavage has remained controversial. Since activated BLM is short-lived (*39, 40*) and thus unsuitable for investigation by NMR spectroscopy or X-ray crystallography, model compounds of activated BLM containing a variety of transition metals have been investigated [reviewed in (*41*)]. NMR studies in the Hecht lab have demonstrated that Zn(II)-BLM can bind DNA in the minor groove (*42, 43*). However, multiple binding motifs and minimal NOE evidence have complicated the interpretation of their studies. Their model fails to adequately describe the chemistry of cleavage and the specificity of cleavage. Since Zn(II)-BLM does not cleave DNA and since it is not known whether Fe(II)-BLM is long-lived enough to reach the nucleus of a cell, it is unclear at this point whether Zn(II)-BLM presents a good structural model for FeBLM.

The most compelling evidence that FeBLM can effect DNA cleavage by a mode other than intercalation has resulted from a recent experiment carried out by Abraham et al. They tethered FeBLM A_5 to a controlled pore glass bead through the bithiazole tail and demonstrated that the tethered FeBLM could effect ss cleavage almost as efficiently as nontethered FeBLM. Presuming the bead is too large to intercalate from the minor groove, an alternate binding mode is required (*44*). However, it is unclear if this tethered FeBLM can effect ds cleavage.

The Otvos and Petering labs, our lab, and more recently the Wang lab have investigated Co(III)-BLM complexes (*38, 45*−*51*). Structural studies have consistently shown that Co(III)-BLM-OOH (CoBLM) complexes bind DNA by partial intercalation (*38, 46*−*48, 50, 51*). CoBLM is a diamagnetic analogue of Fe(III)-BLM-OOH, "activated BLM" (*10*−*12*). This CoBLM cleaves DNA with the same sequence specificity as FeBLM, but only in the presence of light (*52, 53*). Thus, CoBLM has been the analogue of choice in several labs to examine the structural interaction of BLM with DNA (*38, 46*−*48, 50, 51*).

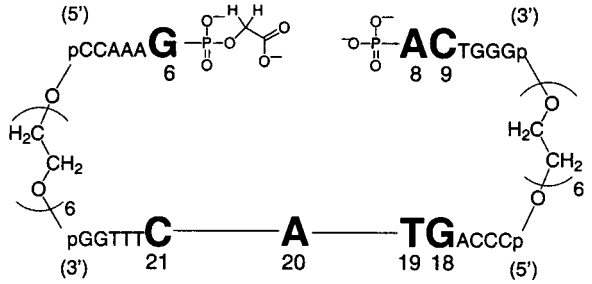

1

FIGURE 5: Schematic drawing of the duplex DNA with the 3′-PG lesion and the 5′-P. The duplex oligonucleotide is constructed as a double hairpin. Hexaethylene glycol spacers connect the two strands of the duplex. These linkers were added to prevent fraying at the ends of the short oligonucleotide pieces. The numbering for the bases of the GTAC box has been provided.

Two-dimensional NMR studies of CoBLM bound to two different DNA sequences have shown that this BLM species binds with the metal binding domain in the minor groove and the bithiazole tail partially intercalated into the helix 3′ to the cleavage site (*38*, *48*). These studies have also provided explanations for the basis of BLM's sequence specificity and chemical specificity.

Our structural model studies and studies on ds cleavage have allowed us to postulate a mechanism for how one molecule of BLM can effect ds cleavage. These studies point to the importance of the rigidity of the metal binding domain and the linker, and to the flexibility of the bithiazole tail relative to other intercalators. The model for ds cleavage involves a 180° rotation about the C−C bond connecting the two thiazolium rings, while the bithiazole tail remains intercalated in the helix. The NMR structures of CoBLM bound to DNA all show a trans relationship of the bithiazole ring protons (*38*, *48*, *50*, *51*). Thus, this rotation would result in a change to a cis conformation. This rotation is followed by a ∼117° rotation around an axis perpendicular to the plane of the bithiazole rings while keeping the ring system coplanar to the DNA base pairs. This conformational change only in the bithiazole tail suffices to reposition the CoBLM metal binding domain from the first cleavage site to the second one, a distance of 15−18 Å, depending on whether the cleavage is staggered or blunt-ended (*38*).

Our studies on FeBLM-mediated ds cleavage led to the discovery of a hot spot for ds cleavage, 5′-GTAC-3′ (*19*). We have used this sequence and built in a 3′-PG and 5′-P lesion at the primary cleavage site to test our model for ds cleavage: the importance of the first lesion and the role of the bithiazole tail of BLM in this process. In this paper, we present a structural model of CoBLM bound to a 3′-PG next to a 5′-P (X) in d(CCAAAGXACTGGG)·d(CCCAGTACTTTGG) (**1**, Figure 5). This duplex oligonucleotide was constructed as a double hairpin with hexaethylene glycol spacers connecting the two strands at G13 to C14 and at C1 to G26 for added stability. The synthesis and structural model of this oligonucleotide will be reported elsewhere (Junker, H.-D., Hoehn, S. T., Bunt, R. C., Turner, C. J., and Stubbe, J., unpublished experiments).

The titration of CoBLM with the lesioned oligonucleotide resulted in formation of a 1:1 complex of the drug bound to the oligonucleotide as monitored by 1D NMR spectroscopy. Two-dimensional NMR methods in conjunction with molecular modeling have provided a structural model of the complex. The hypothesis suggested by Vanderwall et al. (*38*) that ds DNA cleavage by BLM involves rotation about the C−C bond connecting the two BLM thiazolium rings in the tail region is consistent with this model.

MATERIALS AND METHODS

Preparation of the 3′-PG Lesion and of CoBLM. The synthesis and sample preparation of the 3′-PG lesion (**1**, Figure 5) will be reported elsewhere (Junker, H.-D., Hoehn, S. T., Bunt, R. C., Turner, C. J., and Stubbe, J., unpublished experiments). Apo BLM-B_2 was purchased from Cal Biochem. CoBLM was prepared and purified as previously described (*54*).

Titration with CoBLM. CoBLM (12 mM in D_2O) was added to **1** (1.4 mM in 500 μL of D_2O) in small aliquots. After each addition, a 1D NMR spectrum was acquired. Titrations were continued until a 1:1 complex was observed.

NMR Experiments. All NMR experiments were performed on custom-built 600 or 750 MHz NMR spectrometers at the Francis Bitter Magnet Laboratory. The acquired data were transferred to a Silicon Graphics work station and processed using Felix software, version 95, Molecular Simulations Inc. ^{1}H and ^{13}C chemical shifts were referenced to an internal standard, sodium 3-(trimethylsilyl)-1-propanesulfonate (TSP) at 0.00 ppm.

PECOSY, TOCSY (30, 60, or 100 ms mixing times), NOESY (100, 200, and 400 ms mixing times), and ROESY (200 and 400 ms mixing times) experiments were recorded at 750 MHz at 20 °C in D_2O. Data sets of 4096 × 512 complex points were acquired with spectral widths of 8000 Hz in both dimensions and 32 scans per t_1 increment. During the relaxation delay period, a presaturation pulse of 2 s was used for solvent suppression. For NOESY experiments in 90% H_2O/10% D_2O at 5 °C (100, 200, and 400 ms mixing times), a WATERGATE gradient pulse sequence (*55*) was used for water suppression. Data sets with 4096 × 512 complex points were acquired with spectral widths of 15 000 Hz in both dimensions. For all these experiments, spectra were zero-filled to 4096 points in the t_1 dimension. The data were processed with a combination of exponential and Gaussian weighting functions. Baselines were corrected with a polynomial or an automatic baseline correction routine in t_2 when necessary.

The following experiments were all run on the 600 MHz NMR spectrometer at 20 °C in D_2O. A ^{13}C-HSQC experiment was run with a spectral width of 6000 Hz in both dimensions and 4096 × 512 complex points to determine the bithiazole proton chemical shifts. Gradient-enhanced ^{31}P-HSQC (spectral width 6000 × 2000 Hz, 4096 × 128 complex points) and ^{31}P-HCOSY (spectral width 6000 × 2000 Hz, 4096 × 128 complex points) experiments were also carried out (*56*, *57*). The ^{31}P spectra were referenced indirectly through the gyromagnetic ratio to trimethyl phosphate (TMP) by external calibration on TSP (*58*).

Molecular Modeling. (A) Distance Constraints. Distance constraints were derived from a 200 ms NOESY experiment at 750 MHz. Peak volumes were assigned by visual inspection using H2′−H2″ NOEs and cytosine H5−H6 NOEs as

a guide for strong NOEs. NOEs were classified as strong, medium, and weak with distances of 1.7−3.7, 2.5−5.0, and 3.5−6.5 Å, respectively. An additional 0.5 Å was allowed for the upper distance bound for NOEs involving methyl groups. NOE volumes were also calculated with the peak pick protocol in Felix 95, and the measured volumes agreed well with those derived from visual inspection. Hydrogen bonds between base pairs were included as restraints for all of the residues. Overall, 729 experimentally determined NOEs were included in the molecular dynamics calculations.

(B) Dihedral Angle Constraints. Coupling constants for H1′−H2′ and H1′−H2″ were derived from a PECOSY experiment. Dihedral angle constraints consistent with a C2′ endo conformation were used for all residues for which coupling constant information was available. For these residues, the dihedral angle H1′−C1′−C2′−H2″ was set at 26° ± 10°, the dihedral angle H1′−C1′−C2′−H2′ was set at 148° ± 10°, and the dihedral angle H2″−C2′−C1′−O4′ was set at 144° ± 10°. Backbone dihedral angles were set for *n*H3′−*n*C3′−*n*O3′−(*n*+1)P at −80° ± 20°, except at G6 where the angle range was increased to ±40°. Dihedral angles for C4′−C5′−O5′−P were set for all residues at −145° ± 20°, except for residue 8, which was not constrained. A total of 96 dihedral constraints were included in the molecular dynamics calculations.

Building of Initial Coordinate Files. The 3′-PG, 5′-P containing oligonucleotide was initially constructed in InsightII (version 95, Molecular Simulations Inc.) as will be published elsewhere (Junker, H.-D., Hoehn, S. T., Bunt, R. C., Turner, C. J., and Stubbe, J., unpublished experiments). CoBLM (B_2) was also constructed in InsightII based on the coordinates of CoBLM (A_2) (*38*) by replacing the dimethylsulfonium tail with a guanidinium tail. The CoBLM molecule was then docked to **1** with the metal binding domain near the T19 residue as indicated by NOEs between the CoBLM metal binding domain and the protons of T19. The bithiazole tail was partially intercalated between T19 and A20 as indicated by NOEs between the bithiazole protons and DNA residues 8, 19, and 20. The hexaethylene glycol linkers were not included in the molecular dynamics calculations. A second complex of CoBLM bound to the 3′-PG lesion was constructed in InsightII with the bithiazole tail in the minor groove and the metal binding domain again near the T19 residue. Modifications to allow for a 3′-PG in the molecular dynamics calculations were also added in the parameter and topology files of the CHARMm force field (*59*, *60*) used for all subsequent calculations. These modifications will be described in another paper (Junker, H.-D., Hoehn, S. T., Bunt, R. C., Turner, C. J., and Stubbe, J., unpublished experiments). Parameter and topology files based on the CHARMm force field for CoBLM (A_2) were provided by Dr. Dana Vanderwall (Vanderwall, D. E., personal communication) and modified to allow for the guanidinium tail of BLM B_2 (*59*, *60*). The initial atom positions for the 3′-PG−BLM complex built in InsightII were read into XPLOR 3.851 on a Silicon Graphics (SGI) work station. Using the CHARMm force field, the molecular structure file (psf) and the molecular coordinate file (pdb) necessary for the molecular dynamics calculations were constructed for both the partially intercalated and the minor groove bound species.

MD Calculations. All experimental constraints were included in initial minimizations, molecular dynamics trajectories, and final minimizations. Initial coordinates for the partially intercalated complex were energy-minimized at 300 K with 200 steps of conjugate gradient minimization. In vacuo molecular dynamics trajectories were then run for 100 ps at 300 K. Throughout the energy minimizations and molecular dynamics trajectories, planarity constraints were included for atoms in aromatic systems at 200 kcal mol^{-1} $Å^{-2}$. The NOE force constant was 50 kcal mol^{-1} $Å^{-2}$, while the dihedral angle force constant was 100 kcal mol^{-1} rad^{-2}. These force constants were chosen to minimize NOE distance constraint and dihedral angle constraint violations. Nonbonded interactions had a cutoff of 11.5 Å. The nonbonded interaction was switched from on to off between 9.5 and 10.5 Å. During the molecular dynamics calculations, atomic coordinates were written to a trajectory file every 0.2 ps throughout the 100 ps molecular dynamics trajectory. The structure was averaged over the last 10 ps of the run, and the averaged structure was again subjected to 200 steps of conjugate gradient minimization. Ten averaged structures were calculated. These 10 averaged structures were then averaged and minimized with 100 steps of conjugate gradient minimization to yield a final averaged minimized structure used for the back-calculations. Coordinates for the 10 averaged structures (accession no. 1G5L) and the final minimized structure (accession no. 1GJ2) have been deposited in the PDB. As a control experiment, the modeling protocol described above was run 3 times using the initial coordinates of the minor groove bound species. All runs gave qualitatively the same final structure with the bithiazole tail partially intercalated in a fashion similar to the above averaged structure.

Back-Calculations. Back-calculations were performed in InsightII using the Matrix Doubling approach. The entire 200 ms NOESY spectrum at 750 MHz was back-calculated for an average of 10 structures where each structure resulted from a separate 100 ps molecular dynamics run. The spectrum was calculated using the full relaxation matrix with a rotational correlation time (τ_c) of 5 ns.

RESULTS

*Titration of CoBLM with **1** To Form a 1:1 Complex.* CoBLM was titrated with d(CCAAAGXACTGGG)·(CCCAGTACTTTGG) (**1**, Figure 5) and monitored by 1D NMR spectroscopy (Figure 6). The disappearance of the peaks for the free A8 H8 (peak 2, 8.53 ppm) and the T19 H6 (peak 5, 7.15 ppm) in **1**, concomitant with the appearance of new peaks attributed to the complexed T19 H6 (peak 6), A20 H8 (peak 3), and C9 H6 (peak 4), and to the bound CoBLM (peaks 1 and 7), indicated the progress of the titration. This titration revealed that a 1:1 complex is generated in slow exchange on the NMR time scale. In contrast, 1D and 2D NMR studies of an abasic site in the same sequence context, titrated with CoBLM, showed evidence of at least four different conformations for the BLM (Figure 7) (Hoehn, S. T., Turner, C. J., and Stubbe, J., unpublished experiments). This is especially apparent in the region between 6.6 and 7.0 ppm where a single peak would be expected for a 1:1 complex (compare Figure 6c). Instead, at least four peaks of various intensities are detected (Figure 7). Thus, even though the backbone conformations of the free abasic site

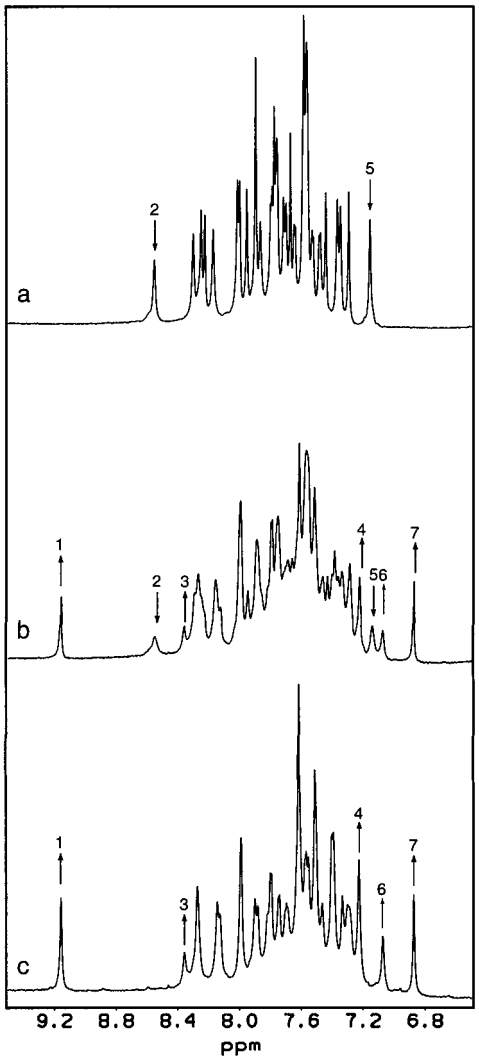

FIGURE 6: Titration of CoBLM with **1** (Figure 5). These 1D NMR spectra at 750 MHz show the progression of the oligonucleotide by itself (a), to 0.45:1 BLM:DNA (b), and to the 1:1 complex of CoBLM with DNA (c). Peaks 1−7 are, in order from left to right, BLM His H2, free A8 H8, complex A20 H8, complex C9 H6, free T19 H6, complex T19 H6, and BLM Bith H5′.

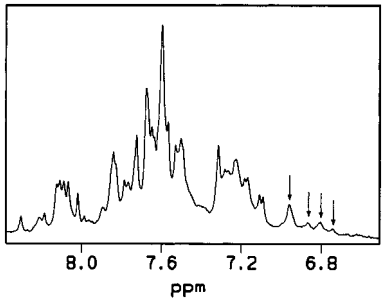

FIGURE 7: Complex of CoBLM and the abasic site containing oligonucleotide. Multiple species are apparent in the region near 6.8 ppm (bithiazole protons) as indicated by arrows. Compare this region to Figure 6c.

containing oligonucleotide and free **1** are similar, as is the extrahelical location of DNA damage (Hoehn, S. T., Junker, H.-D., Bunt, R. C., Turner, C. J., and Stubbe, J., unpublished experiments), binding of CoBLM to **1** is significantly more specific.

Assignment of the Proton Chemical Shifts. Assignment of the chemical shifts of **1** and of CoBLM was achieved by standard methods through NOESY and TOCSY spectroscopy in D_2O (*61*). Comparisons between the chemical shift assignments for the complexed oligonucleotide and free **1** (Junker, H.-D., Hoehn, S. T., Bunt, R. C., Turner, C. J., and Stubbe, J., unpublished experiments) are presented in Tables 1 and 2 of the Supporting Information. Comparisons of the chemical shift assignments between free CoBLM (*54*), CoBLM bound to $d(CCAGTACTGG)_2$ (*38*), and CoBLM bound to **1** are presented in Table 3 of the Supporting Information.

All of the nonexchangeable protons in **1** with the exception of a few H5′/H5″ sugar protons have been assigned. The assignment of the proton chemical shifts for the complexed oligonucleotide was facilitated for C1−A5, G12, G13, C14, C15, and T22−G26 by the prior assignment of the free oligonucleotide (Junker, H.-D., Hoehn, S. T., Bunt, R. C., Turner, C. J., and Stubbe, J., unpublished experiments). Near the putative CoBLM binding region significant chemical shift perturbations were observed for many G18 and T19 protons relative to free **1**. The most striking example of a perturbed chemical shift is the T19 H4′ which was shifted from 4.16 ppm in **1** to 3.24 ppm in the complex. This chemical shift is well outside the envelope of all H4′ chemical shifts in the free oligonucleotide (4.44−4.07 ppm) and is also identical to the one observed for the H4′ of T5 in the d(CCAGTACTGG)$_2$−CoBLM complex (*38*). In this latter case, the structural model positioned the Co 4.7 Å from this proton. Thus, it is likely that the observed upfield shift of the T19 H4′ in our complex is indicative of its proximity to the metal.

Examination of proton chemical shifts in H_2O has also been very informative. No chemical shifts could be assigned to the C21 amino protons or the G6 imino proton. This result suggests that the G6-C21 base pair is rapidly exchanging and more solvent-exposed in comparison with the intact oligonucleotide. Given its proximity to the 3′-PG lesion, this result is not unexpected. Surprisingly, the imino proton of the T19-A8 base pair on the other side of the lesion is detected at 13.16 ppm. The T10 and T19 imino protons (12.85 and 13.16 ppm, respectively; Table 2, Supporting Information) are both upfield-shifted from the remaining T imino protons (14.11−14.25 ppm). The C9 amino protons and the G18 imino proton are also shifted upfield relative to the remaining C amino and G imino protons. The proximity of the bound CoBLM likely perturbs their chemical shifts.

We have previously assigned the protons associated with the 3′-PG moiety of **1** by HSQC spectroscopy (Junker, H.-D., Hoehn, S. T., Bunt, R. C., Turner, C. J., and Stubbe, J., unpublished experiments). In the complex, it was of interest to determine if the 3′-PG interacted in a specific fashion with the CoBLM. Thus, an HSQC experiment was also carried out for the complex. In the case of free and of complexed **1**, the protons associated with the 3′-PG were at 4.23 ppm. No NOEs to these protons were detected either to the oligonucleotide or to the CoBLM.

To establish the conformation of DNA and to aid in its chemical shift assignments, NOE walks were carried out in the base proton to sugar H1′, base proton to sugar H2′/H2″, and base proton to sugar H3′ regions. As can be seen in Figures 8 and 9, connectivity could be achieved for C1−G6, A8−G13, C14−T19, and A20−G26. There is a break in connectivity between T19 and A20. This latter break is

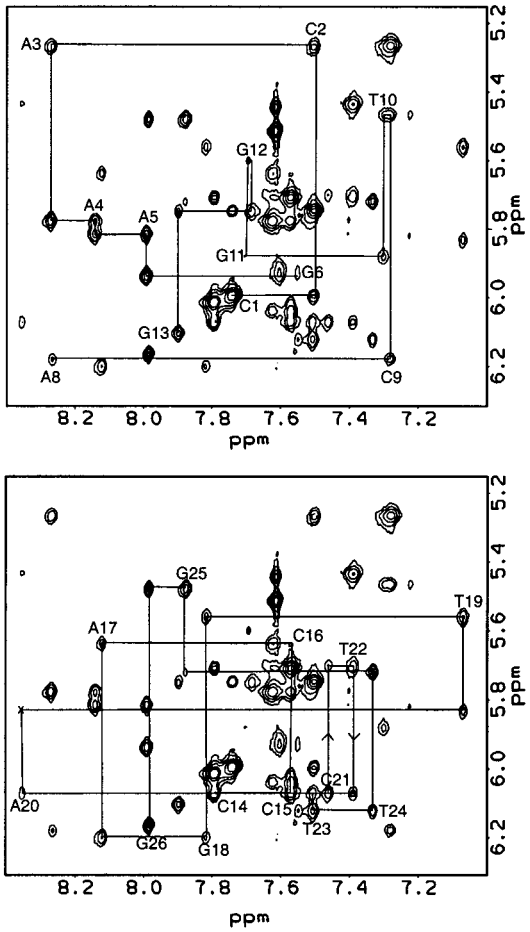

FIGURE 8: NOE walk for a 200 ms mixing time NOESY experiment at 750 MHz. The base proton to H1′ proton region is shown for C1 to G13 (top) and for C14 to G26 (bottom). As expected, there is a break in connectivity at the 3′-PG lesion (between G6 and A8). There is also a break in connectivity between T19 and A20, the putative intercalation site for BLM. This break in connectivity is indicated by x.

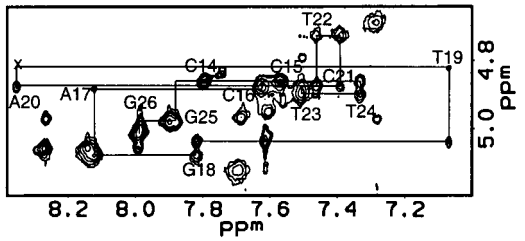

FIGURE 9: Base proton to H3′ proton NOEs at 750 MHz. The NOE walk for the strand opposite the 3′-PG lesion is shown. Connectivity is weak between T24 and G25, but an NOE can be seen at lower contours. There is a complete break in connectivity between T19 and A20 as indicated by x.

expected if CoBLM binds by intercalation 3′ to the cleavage site.

The CoBLM chemical shifts have been assigned based on a wealth of NOE information, as well as TOCSY experiments. A total of 126 NOEs between CoBLM protons were assigned. The chemical shifts assigned for CoBLM bound to **1** are strikingly similar to the ones observed for CoBLM bound to d(CCAGTACTGG)$_2$ (*38*). No significant deviations are observed for the chemical shifts in the metal binding domains of the two complexes (Table 3, Supporting Information). The similarity in chemical shifts suggests that the conformation of the metal binding domain of the CoBLM

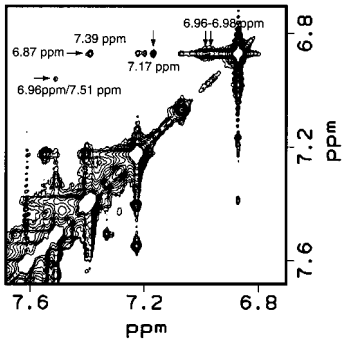

FIGURE 10: NOESY spectrum at 200 ms mixing time of part of the base proton region at 750 MHz. NOEs between the BLM bithiazole H5′ and H5 for two distinct sets of chemical shifts are indicated by horizontal arrows. Exchange peaks between different conformations of the same H5′ or H5 are indicated by vertical arrows. Other NOEs at the H5′ and H5 chemical shifts are between these bithiazole protons and the oligonucleotide protons.

bound opposite the 3′-PG lesion is very similar to the one observed for the intact oligonucleotide.

Assignment of the Bithiazole Ring Protons. To understand the mode of binding of the bithiazole tail, the proton chemical shifts associated with the terminal (H5) and penultimate (H5′) thiazolium ring protons have been assigned. Previous studies have used HSQC spectroscopy to accomplish these assignments (*38*, *48*). A similar experiment has been used to assign the chemical shifts of the major conformations of the bithiazole protons and of the carbons to which these are attached: H5′ to 6.87 and 117.9 ppm, and H5 to 7.51 and 126.9 ppm (Figure 1, Supporting Information). A comparison of the proton chemical shifts with free CoBLM and CoBLM bound to intact oligonucleotide is informative. For free CoBLM, the H5 is at 8.17 ppm and shifts to 6.87 ppm in the intact duplex and to 7.51 ppm in **1**. The H5′ is at 7.82 ppm (free) and shifts to 7.04 ppm (intact) or to 6.87 ppm (**1**). The upfield shifts in CoBLM binding suggest that the bithiazole ring is intercalated and that the penultimate ring bound to **1** is better stacked than in the intact duplex. These data are consistent with the partial intercalative mode of binding suggested by the NOE walks (Figures 8 and 9). A second H5 proton associated with a carbon chemical shift of 127.1 ppm is detected at a much lower contour level in the HSQC spectrum (Figure 1, Supporting Information) and is indicative that there is a second conformation for the terminal thiazolium ring.

Conformations of the Bithiazole Protons. Our model to account for ds cleavage at the second site postulates a rotation around the C−C bond connecting the two thiazolium rings, causing a change in the orientation of the protons from trans to cis (*38*). Having assigned the H5 and H5′ protons (Figure 1, Supporting Information), examination of the 200 ms NOESY spectrum revealed some unexpected results. Cross-peaks were observed between 7.51 and 6.96 ppm, 7.39 and 6.87 ppm, 6.87 and 6.96−6.98 ppm, and 6.87 and 7.17 ppm (Figure 10). These cross-peaks are not associated with the DNA. The population of the species corresponding to the chemical shifts of 6.96−6.98 and 7.17 ppm is sufficiently small that they are undetectable by 1D NMR (7.39 and 7.51 ppm are in a crowded region). At other mixing times, these peaks are also observed, and the cross-peak between 6.87 and 6.96−6.98 ppm also appears in the TOCSY spectra at different mixing times.

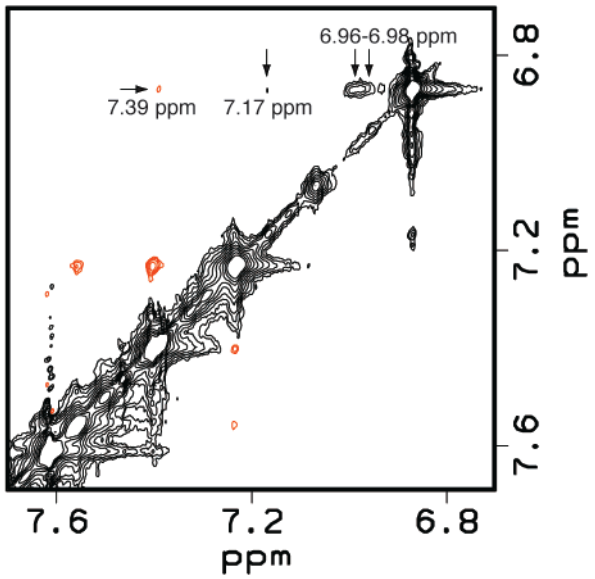

FIGURE 11: ROESY spectrum at 200 ms mixing time of part of the base proton region at 750 MHz. An NOE between the BLM bithiazole H5′ and H5 is indicated by a horizontal arrow. Exchange peaks between different conformations of the same H5′ or H5 are indicated by vertical arrows. NOEs are shown in red (opposite sign as the diagonal); exchange peaks are shown in black (same sign as the diagonal).

One possible explanation for the observed cross-peaks is that they result from two or more species in slow to intermediate exchange on the NMR time scale, that is that they are associated with chemical exchange peaks rather than NOEs. In this scenario, the species with a chemical shift of 7.39 ppm corresponds to a minor conformation of the H5 proton, and the species with chemical shifts of 6.96−6.98 and 7.17 ppm correspond to minor conformations of the H5′ proton. Since there is a broad feature from 6.96 to 6.98 ppm, this peak may be indicative of several closely related conformations rather than a single conformation for the H5′ proton.

A 200 ms mixing time ROESY experiment was carried out to distinguish between NOEs and chemical exchange peaks. This experiment demonstrated that the features connecting 6.87 and 6.96−6.98 ppm, and 6.87 and 7.17 ppm in the NOESY experiment result from exchange interactions between different conformations of the H5′ proton (Figure 11). The nature of these minor conformations cannot be further structurally defined due to their low intensity. Efforts to observe an exchange peak between the major and minor conformations of the H5 proton (at 7.51 and 7.39 ppm, respectively) were unsuccessful, as this peak would be located too close to the diagonal to be detected. Furthermore, no exchange peak was seen between 7.51 ppm and the second minor conformation of the H5 proton (at 7.68 ppm as detected by HSQC spectroscopy) in the ROESY spectrum, possibly because of the low population of the species at 7.68 ppm. As with the conformations resulting in the exchange process observed at 6.96−6.98 and 7.17 ppm, the conformation of the species at 7.68 ppm could not be identified due to its low population. Since the bithiazole tail is bound at the 3′-PG lesion, it is possible that there are several energetically favorable bound conformations, which may differ slightly in the position of the bithiazole rings with respect to the DNA bases. These studies interestingly show

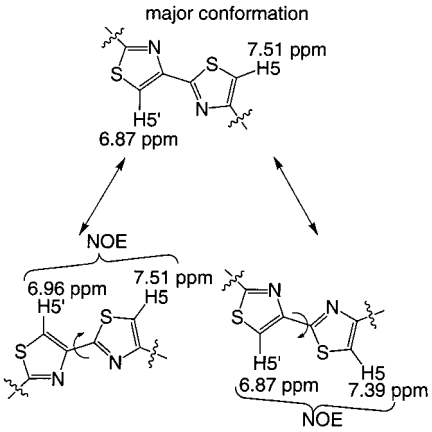

FIGURE 12: Illustration of the ring flipping proposed for the thiazolium rings and the resulting NOEs. The major conformation of the bithiazole protons is trans; no NOE is observed between 6.87 and 7.51 ppm. Chemical shifts of 6.87 and 6.96 ppm describe the same proton as shown by ROESY spectroscopy. Thus, it is plausible that the NOE between 6.96 and 7.51 ppm results from a minor cis conformation in the bithiazole rings. The same is true for the NOE between 6.87 and 7.39 ppm. Each cis conformation can be achieved from the trans configuration by a 180° rotation about the C−C bond connecting the thiazolium rings.

that there are at least two distinct conformations for both the bithiazole H5 and H5′ protons even though a single conformation predominates for each proton.

Orientation of the Bithiazole Protons with Respect to Each Other. The 200 ms mixing time NOESY and ROESY experiments, in addition to showing chemical exchange peaks between different conformations of the same proton, also have revealed the conformation of the thiazolium rings with respect to each other. In the NOESY spectrum (Figure 10), there are weak NOEs between 7.39 and 6.87 ppm and between 7.51 and 6.96 ppm. There is no NOE between 6.87 and 7.51 ppm. ROESY spectroscopy shows that both of these peaks are associated with NOEs and are not chemical exchange peaks (Figures 10 and 11). Since the distance between the bithiazole protons is >6 Å in the trans conformation and ∼5 Å in the cis conformation, an NOE would only be expected if these protons are cis with respect to each other. Since the protons with chemical shifts of 6.87 and 7.51 ppm represent the major conformation of the two thiazolium rings, the trans orientation predominates. However, each bithiazole proton has at least one minor conformation that shows an NOE to the other bithiazole proton in the major conformation. Thus, the protons must be cis with respect to each other, and there are at least two distinct cis conformations for each thiazolium ring (Figure 12). Although the thiazolium rings do not necessarily have to be coplanar, the upfield shifts of both thiazolium protons suggest that the rings are stacked with the DNA bases in an intercalated binding mode. The terminal thiazolium ring would be expected to have much greater flexibility than the penultimate ring. Unfortunately, chemical exchange between the two conformers is undetectable for the technical reasons discussed above.

Structurally Important Exchangeable Protons. One of the most surprising results of the studies of CoBLM bound to the intact GTAC sequence was the detection of the proton associated with the hydroperoxide (*38*, *48*) This proton was stabilized by the DNA and by the linker region of CoBLM,

Table 1: Complete List of NOEs between BLM and **1** at 750 MHz[a]

A8 H2−bith αH*	W	T19 H1′−bith βH*	W	A20 H2−bith H5′	M
A8 H2−bith αH*	W	T19 H1′−val γMe	W	A20 H5′−val αH	W
A8 H2−bith βH*	M	T19 H1′−pyr αH′	W	A20 H5′−val γMe	W
A8 H2−bith βH*	M	T19 H1′−OOH H	M	A20 H5′−thre βMe	M
A8 H2−bith H5′	W	T19 H2′−pyr Me	W	A20 H5′−thre αH	M
A8 H2−bith H5	W	T19 H2″−bith βH*	W	A20 H5′−thre βH	W
A8 H1′−bith H5	W	T19 H3′−OOH H	M	A20 H5″−val γMe	W
A8 H4′−bith H5	W	T19 H4′−bith βH*	M	A20 H5″−thre βMe	W
T10 H1′−ala αH	W	T19 H4′−val γMe	M	A20 H5″−val αH	W
T10 H1′−pyr Hα	W	T19 H4′−pyr Me	M	A20 H5″−thre αH	M
T10 H1′−pyr Hα	M	T19 H4′−val βH	W		
T10 H6−pyr Hα′	W	T19 H4′−pyr βH	W		
G11 H4′−ala αH	M	T19 H6−bith H5′	W		
G11 H4′−ala βH	W	T19 H5″−val γMe	M		
G11 H4′−glu H5	W	T19 H5″−pyr Me	M		
G11 H4′−pyr Hα′	W	T19 H5′−val γMe	M		
G18 H1′−pyr Me	M	T19 H5′−pyr Me	M		
G18 H1′−NH_{2b}	M	T19 H4′−OOH H	S		
G18 H2″−NH_{2b}	M	T19 Me−bith H5′	M		
G18 H4′−pyr Me	M	T19 H3−bith H5′	M		
G18 H5′−pyr Me	M				

[a] Strong, medium, and weak NOEs are indicated by S, M, and W, respectively.

and it exchanged slowly in 90% H_2O/10% D_2O at 5 °C. As expected, this proton showed no direct connectivity with any other proton but exhibited 10 NOEs to the CoBLM and 4 NOEs to the DNA (*38*). A proton at 8.84 ppm was detected in the complex of CoBLM with **1**, a chemical shift identical to that observed in the intact GTAC piece. In the 200 ms mixing time NOESY in 90% H_2O/10% D_2O at 5 °C, this proton showed NOEs of medium intensity to T19 H1′ and T19 H3′ and an NOE of strong intensity to T19 H4′. Four NOEs between this proton and the methylvalerate moiety of the CoBLM were observed as well. The strong NOE between the CoBLM hydroperoxide proton and the T19 H4′ proton in addition to the upfield chemical shift of the H4′ proton suggests that the metal binding domain of CoBLM is bound adjacent to the H4′ of T19, as was also observed for the CoBLM metal binding domain in previous structures with intact oligonucleotides (*38, 48*).

Another proton detected in 90% H_2O/10% D_2O at 5 °C that has important structural implications has been assigned to the 4-amino group of the pyrimidine of CoBLM (Figure 1). Our previous studies showed that this proton was shifted from 7.94 ppm in the free CoBLM to 10.23 ppm in complex with $d(CCAGTACTGG)_2$ (*38*). A similar proton at 10.23 ppm is observed for CoBLM bound to **1**. Our model studies on the complex of intact GTAC with CoBLM attributed this downfield shift to a hydrogen bonding interaction with the N3 of guanine, 5′ to the CoBLM cleavage site. The remarkable similarity in chemical shifts of this unique proton between the intact oligonucleotide and **1** in the presence of CoBLM indicates that this proton is associated with the pyrimidine of CoBLM and is probably forming a similar interaction with G18 in **1**.

BLM Binding Mode. NOEs between the CoBLM and the DNA are required to obtain a structural model of the complex. As can be seen in Table 1, 51 NOEs indicate the location of the CoBLM. Most of these observed interactions involve the metal binding domain of CoBLM, which is located in the minor groove near the T19 deoxyribose. Of the 51 NOEs assigned between the DNA and the CoBLM, 20 involve the T19 residue. The other observed NOEs involve residues T10, G11, G18, and A20 (Table 1).

The bithiazole ring protons show NOEs to protons of residues A8, T19, and A20, located in both the minor and major grooves (e.g., T19 CH_3). It is unlikely that the bithiazole bound in the minor groove would show NOEs to major groove protons. Therefore, these NOE data provide additional support that the bithiazole tail is bound by partial intercalation between T19 and A20.

As indicated above, the chemical shift differences of the H5, H5′ of the bithiazole moiety in the intact oligonucleotides relative to **1** suggested that H5′ of the penultimate thiazolium ring is better stacked in **1**. The difference in the intercalation behavior of the CoBLM with **1** and with the intact GTAC piece can also be seen by ^{31}P NMR (Figure 2, Supporting Information). Our previous studies revealed that when CoBLM is intercalated into the helix in intact oligonucleotides, the ^{31}P chemical shifts near the intercalation site are shifted 1−2 ppm downfield from the envelope of the remaining ^{31}P resonances (*38, 48*). This significant perturbation in ^{31}P chemical shifts is not observed for **1**, probably because the lesion allows for intercalation into the helix with less DNA backbone distortion. Some of the peaks for the resonances are diffuse, indicating increased flexibility of the helix in these regions. Unfortunately, these peaks could not be assigned unambiguously because of spectral overlap.

Molecular Modeling. There is continuing controversy about the binding mode of CoBLM with respect to DNA that leads to DNA cleavage (*44, 62*). Therefore, modeling studies of our complex were performed starting with either a minor groove bound drug or a partially intercalated drug. As indicated in the previous sections, strong evidence based on examination of chemical shifts and NOEs already requires the CoBLM bithiazole tail to intercalate between the T19 and the A20. The averaged structure resulting from 10 separate modeling runs, starting with the bithiazole tail intercalated between T19 and A20, is shown in Figure 13. The 10 structures show a rms deviation of 1.69 Å relative to the average structure (Table 2). Similar modeling experiments in which the bithiazoles were initially positioned in the minor groove gave structural models in which the bithiazoles became intercalated between T19 and A20, similar to the ones starting with the bithiazoles intercalated.

BLM Chemical and Sequence Specificity. FeBLM has long been known to specifically abstract the H4′ proton at a pyrimidine 3′ to guanine. This specificity for the H4′ proton has been explained by model structures of CoBLM bound to a number of intact oligonucleotides (*38, 48*), where the distance between the distal oxygen of the hydroperoxide and the pyrimidine H4′ of the cleavage site has been observed to be short (∼2.5 Å). This short distance between the deoxyribose H4′ proton and the distal oxygen of the hydroperoxide of CoBLM is also seen for CoBLM bound to **1** (2.2 ± 0.2 Å in the averaged structure) (Figure 3, Supporting Information). Since H4′ hydrogen atom abstraction occurs for both ss and ds cleavage events mediated by FeBLM, this short distance is consistent with the observed FeBLM chemistry (*36*).

The structure of CoBLM bound to intact oligonucleotides provided an explanation for BLM's sequence-specificity: cleavage at pyrimidines 3′ to guanines (*38, 48*). As seen in our two previously published structures, two hydrogen bonding interactions between the CoBLM pyrimidine moiety and the guanine 5′ to the cleavage site were inferred by the

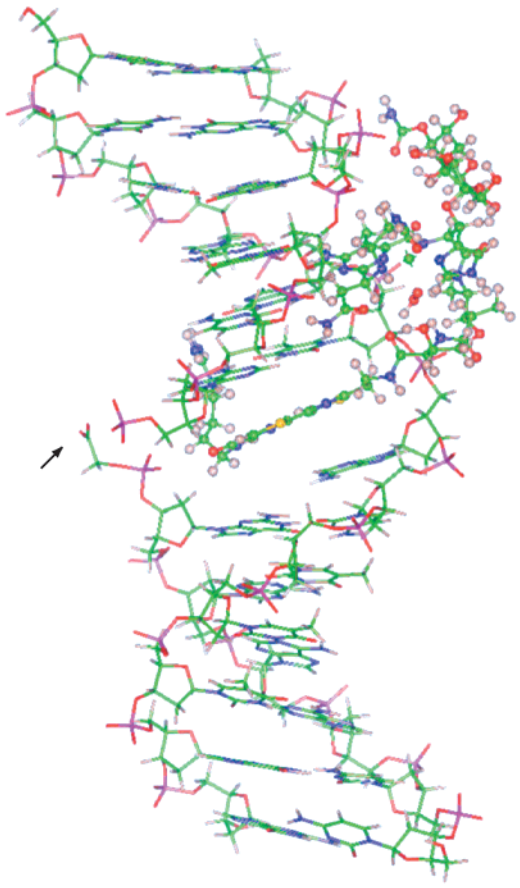

FIGURE 13: Average minimized structure for 10 separate molecular modeling runs. The BLM is shown in ball-and-stick. The metal binding domain of the BLM is located in the minor groove near the T19 deoxyribose, and the bithiazole tail is partially intercalated into the DNA helix. The 3′-PG is indicated by an arrow.

Table 2: Summary of Molecular Modeling Results

	10 structures
rms deviation to av structure for all atoms (Å)	1.69
total no. of distance constraints	729
distance constraints between BLM and DNA	51
distance constraints BLM, intramolecular	126
distance constraints DNA, intramolecular	552
av NOE violation (Å)	0.06
av dihedral angle violation (deg)	1.4
av no. of NOE violations greater than 0.5 Å	0
av no. of dihedral angle violations greater than 5°	0

short distance between the pyrimidine 4-amino group and the N3 of the guanine, and between the pyrimidine N3 and the guanine 2-amino group. In the average structure, the distance between the CoBLM pyrimidine amino group and the N3 of the G18 is 1.86 Å, and the distance between the 2-amino group of G18 and the CoBLM pyrimidine N3 is 2.17 Å (Figure 4, Supporting Information). Even though these distances are comparable to the ones previously observed, the angles for these hydrogen bonds are different (146° and 156°, respectively).

Preorganization of the Linker Region. In collaboration with the Boger lab, the importance of the linker region has been investigated with respect to ds cleavage. The threonine and valerate moieties have been demonstrated to be important in preorganizing the BLM into a compact structure (*62*−*65*). In our ds cleavage model, this preorganization is important in the BLM reorganization to the second cleavage site. Comparing the structure of the CoBLM linker region bound to d(CCAGTACTGG)$_2$ with that bound to **1** shows that they are nearly identical. The rms deviation in the atom positions in these two moieties is only 0.29 Å. This result strongly suggests that the preorganization is important at both the primary and the secondary cleavage site.

Back-Calculation of the Average Minimized Structure. To demonstrate the quality of the model structure relative to the experimental data, the structure was back-calculated. The 200 ms mixing time NOESY spectrum from the average minimized structure is in reasonable agreement with the experimental data (Figure 5, Supporting Information). For the base proton to H1′ region, only minor deviations are seen. The back-calculated spectrum shows all the key features of the experimental data, including the break in connectivity between T19 and A20. The back-calculated spectrum also accurately reflects the intensities of the experimental NOE peaks between the T19 deoxyribose protons and the CoBLM protons. This agreement between the back-calculated spectrum and experimental data supports our structural model presented in Figure 13.

DISCUSSION

Double-strand cleavage has been implicated as a major contributing factor in BLM cytotoxicity (*27*−*29*). Therefore, understanding the mechanism of this process is of significant importance. The Povirk lab has shown that BLM-induced ss and ds DNA damage of reconstituted nucleosomes was inhibited to the same extent in comparison with naked DNA. This result suggested that a single binding event was responsible for both ss and ds cleavage processes. Furthermore, the pattern of inhibition observed suggested an intercalative mode of binding in both processes (*66*).

Our model for ds cleavage based on biochemical studies with FeBLM (*19*) and 2D NMR (*38*) studies of CoBLM bound to a hot spot for ds cleavage is similar to that of Povirk. The availability of structural information, however, has allowed us to put forth a molecular model describing the ds cleavage process (*38*). The key to this model is the rigidity of the metal binding domain and the linker of BLM and the flexibility of the bithiazole tail. Our model proposes that damage occurs at the primary cleavage site. The increased flexibility of the DNA at this lesion site, in conjunction with a low barrier to rotation around the carbon−carbon bond connecting the two thiazolium rings of BLM (Figure 1), allows reorganization of the metal binding domain and the linker to the second strand or dissociation. The ratio of the rate constants for reorganization versus dissociation from the first strand, prior to reorganization, governs the propensity for ds cleavage from the same initial binding mode. This model provides an explanation of the choice of the bithiazole versus a "more proficient intercalator" to assist in DNA binding. The key role of the bithiazole is to orchestrate ds cleavage.

Our model specifically predicted that the metal binding domain of BLM would interact with guanine on the second strand, 5′ to the cleavage site on the first strand. It further predicted that the trans orientation of the H5−H5′-bithiazole protons present when cleavage occurs on the first stand would become cis upon reorganization. Studies of the "lesioned" duplex **1** titrated with CoBLM support the feasibility of this model.

Our NMR data reveal evidence for at least two different conformations of both thiazolium rings. Our findings are consistent with an interconversion between a major species where the protons of the bithiazole moiety are trans with respect to each other, and two distinct minor species where the protons of the bithiazole moiety are cis with respect to each other (Figure 12). In addition, at least one other unidentified minor conformation exists. Presently we cannot rule out the possibility that the bithiazole tail binds in a minor cis conformation rather than in the major trans conformation. However, ROESY experiments show that the two conformations can interconvert while the BLM is bound to the DNA. This interconversion is required for our mechanism of ds cleavage and demonstrates the feasibility of our proposal.

Precedence on the NMR time scale for ring flipping of aromatic systems while intercalated in the DNA helix has been provided in recent studies of the antitumor drug bisnaphthalimide LU-79553. Gallego et al. reported that each intercalated naphthalimide chromophore (*67*) has two different conformational states that interconvert by ring flipping with an exchange rate of 1800 s^{-1} at 36 °C (20 s^{-1} at 2 °C), while remaining intercalated in the helix. The activation energy for this flipping was determined to be 22 kcal mol^{-1} (*67*). This flipping of the aromatic moieties is similar to our model for the role of the bithiazole moiety in ds cleavage. The 180° rotation of the thiazolium rings is energetically possible, as the barrier to rotation about the C−C bond connecting these rings in an unsubstituted 2,4′-bithiazole has been calculated as ≤7.5 kcal by extended Hückel theory (*68*). Flipping of the thiazolium rings of BLM while partially intercalated in the helix is, therefore, precedented based on the low barrier to rotation and the results of Gallego et al. Thus, our NMR data support the required flexibility of the bithiazole tail in the ds cleavage process.

Other antitumor drugs also show ring flipping of aromatic systems while bound to DNA. Protons of the phenyl ring of Hoechst 33258 are observed to be in fast exchange on the NMR time scale, while the entire molecule remains bound in the minor groove in slow to intermediate exchange (*69*−*71*).

The recognition element that causes BLM to reorganize from one cleavage site to the next is not understood. We have postulated that it involves the 3′-PG, 5′-P lesion or a precursor to this lesion, as have other labs (*72*). Such lesions are known to increase the flexibility of DNA in the region of the lesion and could thus facilitate this process. Base propenal release ($t_{1/2}$ of 6.7 ± 0.3 min) (Figure 3) under certain conditions is slower than either ss or ds DNA cleavage (*73*, *74*), so it is possible that the trigger for reorganization includes the 3′-PG end, and the base of the target pyrimidine still attached to the 5′ end (*72*). Since this precursor to the 3′-PG and the base propenal is chemically unstable, it does not lend itself to investigation by 2D NMR spectroscopy. We have thus focused on the interaction of **1** with CoBLM.

Insight into the effect of lesions on BLM's ability to cleave DNA previously has been investigated in an effort to shed additional light on the ds cleavage process (*72*, *75*). Keller and Oppenheimer generated one-base gaps with 3′- and 5′-phosphate ends surrounding the gap. They showed that in some sequences, these gaps induced breaks at the second strand with 3′ one-base overhangs, a cleavage pattern thus far not observed for BLM-induced ds cleavage (*19*, *25*). However, these charged gaps were much better at directing BLM to the second cleavage site than were gaps containing 3′- and/or 5′-hydroxyl ends (*75*).

Since the Keller and Oppenheimer model did not account for the ds cleavage specificity of BLM in several instances, Charles and Povirk investigated a model containing a nick, rather than a gap, namely, a 3′-OH and an intact deoxyribose at the 5′ side (*72*). For this type of lesion, cleavage efficiency at the underlined secondary cleavage site 5′-G<u>G</u>CG-3′ was increased by 50% over the intact duplex. Substituting a PG at the 3′ position of the nicked duplex showed no increase in cleavage efficiency at this site.

Even though the DNA species directing the BLM to the second cleavage site may involve a fragment of the first deoxyribose and the base attached to the 5′ end, a 3′-PG end next to a 5′-P end is sufficient to direct the BLM to the second cleavage site. Studies of **1** with CoBLM showed cleavage only at T19 (Bunt, R. C., and Stubbe, J., unpublished experiments).

Our studies demonstrate that the 3′-PG end next to a 5′-P end also facilitates binding of CoBLM at the lesion in a single predominant mode (Figure 13). Thus, it is striking that similar studies with an abasic site lesion of **1** generated multiple binding modes (Figure 7). These results are consistent with the model for ds cleavage that requires the 3′-PG pathway. Recall that ds cleavage is not observed with the 4′-ketoabasic site lesion at the primary cleavage site (Figure 3). In addition to the PG pathway being required for reactivation of BLM, it also may be essential for reorganization, flexibility, and appropriate BLM binding to the uncleaved strand. No direct NOE evidence for the interaction of the 3′-PG with the CoBLM, however, was found.

FeBLM-induced ds cleavage of the GTAC sequence leads to a 3′ staggered end (Figure 4). However, in a different sequence context, FeBLM can also lead to blunt-end cleavage (Figure 4). Our model for ds cleavage, however, does accommodate reorganization to the second strand for either staggered-end or blunt-end ds cleavage although the former appears more favorable. In the limited sequence space examined to date, the second cleavage event in both blunt-end and staggered-end ds cleavage often shows a guanine immediately 5′ to the secondary cleavage site (*18*, *19*). It is possible that the BLM recognition motif for the guanine 5′ to the cleavage site, determined for primary cleavage sites in our previous structural studies (*38*, *48*), extends to secondary cleavage sites as well. Hydrogen bonding interactions between the guanine and CoBLM could once again direct and potentiate cleavage at the second site. This proposal is justified as from the 32 ds cleavage sites thus far identified, 19 possess a guanine and another 9 have an adenine in this position (*18*, *19*, *25*). The sequence specificity of ds cleavage established by Povirk (*25*) (Figure 4) and extended by Absalon et al. (*19*) needs to be elaborated on by the investigation of additional sequence space. New methods are required to identify additional hot spots for ds cleavage such as GTAC and to make kinetic measurements of dissociation of BLM relative to reorganization and secondary site cleavage.

SUMMARY

Our studies of CoBLM bound to **1** provide further support for how a single FeBLM can mediate ds cleavage. Our studies support the unique role of the bithiazole tail in the cleavage process and the importance of the guanine 5′ to the cleavage site. The studies further support our model that BLM is a finely tuned machine with the whole being much more efficient than the sum of its parts.

ACKNOWLEDGMENT

We thank Dr. Dana Vanderwall for providing the topology and parameter files for the BLM molecule that were used in the molecular modeling.

SUPPORTING INFORMATION AVAILABLE

Proton chemical shift assignments for **1** and Co(III)-BLM-OOH, in complex and free. ^{13}C-HSQC spectrum at 600 MHz. ^{31}P-HSQC spectrum at 600 MHz. Structural evidence for chemical specificity of CoBLM for the H4′ atom of T19 and for the recognition of guanine by BLM. Comparison between a 200 ms mixing time NOESY spectrum at 750 MHz and a back-calculated 200 ms mixing time NOESY spectrum (8 pages). This material is available free of charge via the Internet at http://pubs.acs.org.

REFERENCES

1. Umezawa, H. (1965) *Antimicrob. Agents Chemother. 5*, 1079−1085.
2. Umezawa, H., Maeda, K., Takeuchi, T., and Okami, Y. (1966) *J. Antibiot. (Tokyo) 19*, 200−209.
3. Hecht, S. M. (1979) *Bleomycin: Chemical, Biochemical, and Biological Aspects*, Springer-Verlag, New York.
4. Umezawa, H. (1980) in *Anticancer agents based on natural product models* (Cassady, J. M., and Douros, J., Eds.) pp 147−166, Academic Press, New York.
5. Sikic, B. I., Rozencweig, M., and Carter, S. K. (1985) *Bleomycin Chemotherapy*, Academic Press, Orlando, FL.
6. Mir, L. M., Tounekti, O., and Orlowski, S. (1996) *Gen. Pharmacol. 27*, 745−748.
7. Lazo, J. S., Sebti, S. M., and Schellens, J. H. (1996) *Cancer Chemother. Biol. Response Modif. 16*, 39−47.
8. Montoto, S., Camos, M., Lopez-Guillermo, A., Bosch, F., Cervantes, F., Blande, J., Esteve, J., Cobo, F., Nomdedeu, B., Campo, E., and Montserrat, E. (2000) *Cancer 88*, 2142−2148.
9. Soulie, P., Garrino, C., Bensmaine, M. A., Bekradda, M., Brain, E., Di Palma, M., Goupil, A., Misset, J. L., and Cvitkovic, E. (1999) *J. Cancer Res. Clin. Oncol. 125*, 707−711.
10. Sausville, E. A., Stein, R. W., Peisach, J., and Horwitz, S. B. (1978) *Biochemistry 17*, 2746−2754.
11. Sausville, E. A., Peisach, J., and Horwitz, S. B. (1976) *Biochem. Biophys. Res. Commun. 73*, 814−822.
12. Sam, J. W., Tang, X. J., and Peisach, J. (1994) *J. Am. Chem. Soc. 116*, 5250−5256.
13. Giloni, L., Takeshita, M., Johnson, F., Iden, C., and Grollman, A. P. (1981) *J. Biol. Chem. 256*, 8608−8615.
14. Stubbe, J., and Kozarich, J. W. (1987) *Chem. Rev. 87*, 1107−1136.
15. D'Andrea, A. D., and Haseltine, W. A. (1978) *Proc. Natl. Acad. Sci. U.S.A. 75*, 3608−3612.
16. Takeshita, M., Grollman, A. P., Ohtsubo, E., and Ohtsubo, H. (1978) *Proc. Natl. Acad. Sci. U.S.A. 75*, 5983−5987.
17. Takeshita, M., Kappen, L. S., Grollman, A. P., Eisenberg, M., and Goldberg, I. H. (1981) *Biochemistry 20*, 7599−7606.
18. Steighner, R. J., and Povirk, L. F. (1990) *Proc. Natl. Acad. Sci. U.S.A. 87*, 8350−8354.
19. Absalon, M. J., Kozarich, J. W., and Stubbe, J. (1995) *Biochemistry 34*, 2065−2075.
20. Povirk, L. F., Wubter, W., Kohnlein, W., and Hutchinson, F. (1977) *Nucleic Acids Res. 4*, 3573−3580.
21. Bradley, M. O., and Kohn, K. W. (1979) *Nucleic Acids Res. 7*, 793−804.
22. Mirabelli, C. K., Huang, C. H., and Crooke, S. T. (1980) *Cancer Res. 40*, 4173−4177.
23. Mirabelli, C. K., Huang, C. H., Fenwick, R. G., and Crooke, S. T. (1985) *Antimicrob. Agents Chemother. 27*, 460−467.
24. Povirk, L. F., and Houlgrave, C. W. (1988) *Biochemistry 27*, 3850−3857.
25. Povirk, L. F., Han, Y. H., and Steighner, R. J. (1989) *Biochemistry 28*, 5808−5814.
26. Lloyd, R. S., Haidle, C. W., and Robberson, D. L. (1978) *Biochemistry 17*, 1890−1896.
27. Byrnes, R. W., and Petering, D. H. (1994) *Radiat. Res. 137*, 162−170.
28. Povirk, L. F., and Goldberg, I. H. (1987) *Biochimie 69*, 815−823.
29. Povirk, L. F. (1996) *Mutat. Res. 355*, 71−89.
30. Magliozzo, R. S., Peisach, J., and Ciriolo, M. R. (1989) *Mol. Pharmacol. 35*, 428−432.
31. Carter, B. J., de Vroom, E., Long, E. C., van der Marel, G. A., van Boom, J. H., and Hecht, S. M. (1990) *Proc. Natl. Acad. Sci. U.S.A. 87*, 9373−9377.
32. Holmes, C. E., and Hecht, S. M. (1993) *J. Biol. Chem. 268*, 25909−25913.
33. Murugesan, N., and Hecht, S. M. (1985) *J. Am. Chem. Soc. 107*, 493−500.
34. Hecht, S. M. (2000) *J. Nat. Prod. 63*, 158−168.
35. Burger, R. M. (1998) *Chem. Rev. 98*, 1153−1169.
36. Absalon, M. J., Wu, W., Kozarich, J. W., and Stubbe, J. (1995) *Biochemistry 34*, 2076−2086.
37. Rashid, R., Langfinger, D., Wagner, R., Schuchmann, H. P., and Von Sonntag, C. (1999) *Int. J. Radiat. Biol. 75*, 101−109.
38. Vanderwall, D. E., Lui, S. M., Wu, W., Turner, C. J., Kozarich, J. W., and Stubbe, J. (1997) *Chem. Biol. 4*, 373−387.
39. Burger, R. M., Peisach, J., and Horwitz, S. B. (1981) *J. Biol. Chem. 256*, 11636−11644.
40. Kuramochi, H., Takahashi, K., Takita, T., and Umezawa, H. (1981) *J. Antibiot. (Tokyo) 34*, 576−582.
41. Claussen, C. A., and Long, E. C. (1999) *Chem. Rev. 99*, 2797−2816.
42. Manderville, R. A., Ellena, J. F., and Hecht, S. M. (1995) *J. Am. Chem. Soc. 117*, 7891−7903.
43. Sucheck, S. J., Ellena, J. F., and Hecht, S. M. (1998) *J. Am. Chem. Soc. 120*, 7450−7460.
44. Abraham, A. T., Zhou, X., and Hecht, S. M. (1999) *J. Am. Chem. Soc. 121*, 1982−1983.
45. Xu, R. X., Nettesheim, D., Otvos, J. D., and Petering, D. H. (1994) *Biochemistry 33*, 907−916.
46. Mao, Q., Fulmer, P., Li, W., DeRose, E. F., and Petering, D. H. (1996) *J. Biol. Chem. 271*, 6185−6191.
47. Wu, W., Vanderwall, D. E., Stubbe, J. A., Kozarich, J. W., and Turner, C. J. (1994) *J. Am. Chem. Soc. 116*, 10843−10844.
48. Wu, W., Vanderwall, D. E., Turner, C. J., Kozarich, J. W., and Stubbe, J. (1996) *J. Am. Chem. Soc. 118*, 1281−1294.
49. Lui, S. M., Vanderwall, D. E., Wu, W., Tang, X. J., Turner, C. J., Kozarich, J. W., and Stubbe, J. (1997) *J. Am. Chem. Soc. 119*, 9603−9613.
50. Caceres-Cortes, J., Sugiyama, H., Ikudome, K., Saito, I., and Wang, A. H. (1997) *Biochemistry 36*, 9995−10005.
51. Caceres-Cortes, J., Sugiyama, H., Ikudome, K., Saito, I., and Wang, A. H. (1997) *Eur. J. Biochem. 244*, 818−828.
52. Chang, C. H., and Meares, C. F. (1984) *Biochemistry 23*, 2268−2274.
53. Chang, C. H., and Meares, C. F. (1982) *Biochemistry 21*, 6332−6334.
54. Wu, W., Vanderwall, D. E., Lui, S. M., Tang, X. J., Turner, C. J., Kozarich, J. W., and Stubbe, J. (1996) *J. Am. Chem. Soc. 118*, 1268−1280.

55. Sklenar, V., Piotto, M., Leppik, R., and Saudek, V. (1993) *J. Magn. Reson., Ser. A 102*, 241−245.
56. Chary, V. V. R., Rastogi, V. K., and Govil, G. (1993) *J. Magn. Reson., Ser. B 102*, 81−83.
57. Sklenar, V., Miyashiro, H., Zon, G., Miles, H. T., and Bax, A. (1986) *FEBS Lett. 208*, 94−98.
58. Markley, J. L., Bax, A., Arata, Y., Hilbers, C. W., Kaptein, R., Sykes, B. D., Wright, P. E., and Wuthrich, K. (1998) *J. Mol. Biol. 280*, 933−952.
59. MacKerell, A. D., Wiorkiewiczkuczera, J., and Karplus, M. (1995) *J. Am. Chem. Soc. 117*, 11946−11975.
60. MacKerell, A. D., Bashford, D., Bellott, M., Dunbrack, R. L., Evanseck, J. D., Field, M. J., Fischer, S., Gao, J., Guo, H., Ha, S., Joseph-McCarthy, D., Kuchnir, L., Kuczera, K., Lau, F. T. K., Mattos, C., Michnick, S., Ngo, T., Nguyen, D. T., Prodhom, B., Reiher, W. E., Roux, B., Schlenkrich, M., Smith, J. C., Stote, R., Straub, J., Watanabe, M., Wiorkiewicz-Kuczera, J., Yin, D., and Karplus, M. (1998) *J. Phys. Chem. B 102*, 3586−3616.
61. Wijmenga, S. S., Mooren, M. W., and Hilbers, C. W. (1993) in *NMR of Macromolecules: a Practical Approach* (Roberts, G. C. K., Ed.) pp 217−283, Oxford University Press, Oxford, U.K.
62. Stubbe, J., Kozarich, J. W., Wu, W., and Vanderwall, D. E. (1996) *Acc. Chem. Res. 29*, 322−330.
63. Boger, D. L., Ramsey, T. M., Cai, H., Hoehn, S. T., and Stubbe, J. A. (1998) *J. Am. Chem. Soc. 120*, 9139−9148.
64. Boger, D. L., Ramsey, T. M., Cai, H., Hoehn, S. T., and Stubbe, J. (1998) *J. Am. Chem. Soc. 120*, 9149−9158.
65. Boger, D. L., and Cai, H. (1999) *Angew. Chem., Int. Ed. Engl. 38*, 449−476.
66. Smith, R. L., Bauer, G. B., and Povirk, L. F. (1994) *J. Biol. Chem. 269*, 30587−30594.
67. Gallego, J., and Reid, B. R. (1999) *Biochemistry 38*, 15104−15115.
68. Bouscasse, L., Bouin, D., Baudrion, C., and Aune, J. P. (1993) *Spectrosc. Lett. 26*, 1889−1900.
69. Embrey, K. J., Searle, M. S., and Craik, D. J. (1993) *Eur. J. Biochem. 211*, 437−447.
70. Fede, A., Labhardt, A., Bannwarth, W., and Leupin, W. (1991) *Biochemistry 30*, 11377−11388.
71. Searle, M. S., and Embrey, K. J. (1990) *Nucleic Acids Res. 18*, 3753−3762.
72. Charles, K., and Povirk, L. F. (1998) *Chem. Res. Toxicol. 11*, 1580−1585.
73. Burger, R. M., Projan, S. J., Horwitz, S. B., and Peisach, J. (1986) *J. Biol. Chem. 261*, 15955−15959.
74. Burger, R. M., Drlica, K., and Birdsall, B. (1994) *J. Biol. Chem. 269*, 25978−25985.
75. Keller, T. J., and Oppenheimer, N. J. (1987) *J. Biol. Chem. 262*, 15144−15150.

BI002635G